

A facet-based numerical model to retrieve ice sheet topography from Sentinel-3 altimetry

Supplementary materials

Section S1: Description of the numerical facet-based model (section 2)

<i>Symbol</i>	<i>Parameter</i>	<i>Value</i>
c	Speed of light	299792458 m s ⁻¹
F_c	Carrier Frequency	13.575 GHz
G_0	One way antenna gain	42 dB
θ_{3dB}	Antenna beamwidth at -3dB	1.35°
σ_0	Backscatter coefficient	6 dB
BW	Received bandwidth	320 MHz
R_{ref}	Tracker range reference	43 (index in the window analysis)
N_w	Number of samples in the window analysis	128 range gates
N_{ew}	Number of samples in the extended window analysis	512 range gates
FP_s	DEM surface extracted around nadir	35 km

Table S1: Input parameters of the numerical model. Note: the satellite and nadir positions and the altimeter tracker ranges are read in the ESA L2 Products.

The following figure shows the conceptual flow chart of the facet-based simulation module, described in section 2.2:

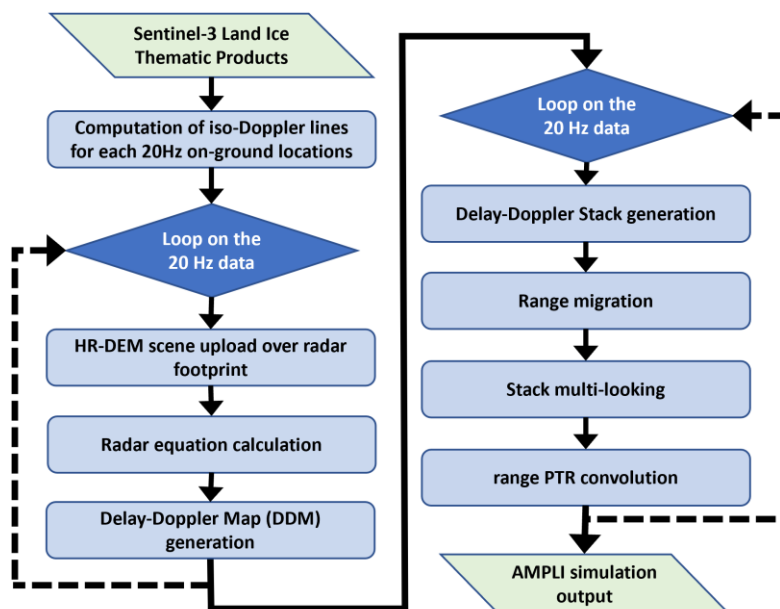


Figure S1: Flow chart of the facet-based simulation module implemented in AMPLI.

a) Pre-processing

The AMPLI software takes as input a level-2 Sentinel-3 Land Ice Thematic Products, Baseline Collection n°5. The software processes separately and independently each equator-to-equator track disseminated by ESA in the Copernicus Data Space Ecosystem (770 tracks per radar cycle of 27 days).

<https://dataspace.copernicus.eu/>

During a pre-processing procedure, the 20 Hz records located over the Antarctic ice sheet and ice shelves are selected, using the surface mask from BedMachine dataset, version n°3 for Antarctica (Morlinghem et al., 2020).

b) Iso-Doppler lines computation

For each 20 Hz record, we determine a vector of points distributed in the cross-track direction, sampled at 10 m, and extending up to ± 15 km from nadir. These points correspond to iso-Doppler lines, that are further used to reproduce the delay-Doppler beams, as explained in step (d). They are illustrated in the main text in Fig. 1, annotated as “iso-Doppler frequencies” (plotted in cyan colour).

c) Radar equation calculation

A loop is performed on the 20 Hz measurements. For each of them, a 35 km x 35 km area of the REMA mosaic DEM (version 2.0, 10 m resolution) is read. The extracted matrix is centred around nadir location. The energy backscattered at snow-air interface $P_{fs}(x,y)$ is computed for each facet of the 35 km x 35 km DEM, according to the Brown model (Brown, 1977). All equations are adapted to account for a spherical Earth. The geometrical computations are performed in the Antarctic Polar Stereographic projection (EPSG:3031).

$$P_{fs}(x,y) = \frac{\lambda \sigma_0}{(4\pi)^3} \int_A \left(\frac{G^2(\theta)}{r^4} \right) dA \quad (1)$$

where:

➤ λ is the radar wavelength = $\frac{c}{Fc}$

➤ r is the distance between antenna and the facet

$$r(x,y) = \sqrt{dx^2 + dy^2 + dz^2} \quad (2)$$

dx and dy are the horizontal distances between nadir and the DEM facet, calculated with the cartesian stereographic coordinates.

dz is the vertical distance between the satellite altitude and the facet height.

➤ $G(\theta)$ the antenna pattern modelled with a Gaussian function:

$$G(\theta) = G_0 e^{-\frac{2}{\gamma} \sin^2 \theta} \quad \text{with } \gamma = \frac{2 \sin^2 \frac{\theta_{3dB}}{2}}{\ln(2)} \quad (3)$$

θ being the angle from the antenna boresight axis to the line from the sensor to dA . θ_{3dB} is the antenna beamwidth at -3 dB.

➤ σ_0 is the backscattering coefficient, per unit scattering area

σ_0 is taken as a constant (= 6 dB). We neglect the σ_0 variation with angle of incidence, by making the assumption that the impact remains relatively minor compared to the antenna aperture. This assumption can be taken, based on the relative homogeneity of the ice sheet surface (at the footprint scale), in terms of backscattering properties. Brown (1977) also took this assumption for the ocean surface.

- **A is the area of a surface facet** (constant set to 1 for the sake of simplicity)

In addition, a range index R_i is attributed to the facets, given the satellite-facet distance and the on-board tracker command, according to:

$$R_i(x, y) = \left(\frac{r - Tr}{\alpha} \right) + R_{ref} \quad (4)$$

Where:

α is the altimeter vertical resolution = $\frac{c}{2 Bw}$

T_r the altimeter tracker range, variable “*tracker_range_20_ku*” in the ESA L2 product. In order to use the initial tracker range of the altimeter, the offset applied in the PDGS during the delay-Doppler processing with extended window is removed (variable “*range_shift_waveform_20_ku*” in the ESA L2 product).

R_{ref} the reference index of the tracker range in the window analysis.

d) Delay-Doppler map generation

As mentioned in the main text, DDMs are constructed by integrating the energy $P_{fs}(x, y)$, given the facet-satellite distance in slant range (range-time domain, t), and in along-track (Doppler frequency domain, f).

In the ESA PDGS, the on-ground spacing of the “*lat_20_ku*” and “*lon_20_ku*” coordinates are determined based on the delay-Doppler along-track resolution. Thus, two consecutive 20 Hz measurements are separated by ~330 m on-ground (slightly varying along the track with satellite altitude and velocity). We take advantage of this configuration to simulate the Delay-Doppler Maps (DDM) at every 20 Hz record. For each of the 20 Hz points, the 31 previous and 32 next “*lat_20_ku*” and “*lon_20_ku*” coordinates are selected and considered as central positions of the 64 delay-Doppler beams (the case of data gap within a track is handled). The 64 delay-Doppler beams constituting the DDM are computed by integrating the backscattered energy P_{fs} along the 64 corresponding iso-Doppler lines, determined in (b), and sorted in range gate according to R_i value.

Following ESA PDGS approach, we calculate first the DDMs along the track. The delay-Doppler stacks are generated in a second step, described in (e). In addition, for each of the 64 delay-Doppler beams of the DDM (f, t), a histogram of the energy backscattered is constructed, as a function of:

- ❖ the slant-range distance between the facet and the satellite (t)
- ❖ the cross-track distance between the facet and the ground track (u)

This signal is called the Cross-Track Backscatter Distribution: CTBD (f, t, u), and is further used in the relocation processing.

e) Delay-Doppler stack generation

A second loop is performed on the 20 Hz records. The delay-Doppler stacks are generated following the PDGS architecture:

- The delay-Doppler stack is constructed by gathering the delay-Doppler beams from different DDM. These beams sample the same delay-Doppler footprint on-ground, therefore from different look angles along the satellite track. As mentioned in the main text, the simulated stacks include 45 single looks (available at 20 Hz rate) to be consistent with the PDGS (180 single looks collected, generated at 80 Hz rate).
- Before range migrations, the window analysis is extended from 128 to 512 samples
- Range migrations are applied to align the single looks together in the extended window analysis. The migrations include the slant range ones, as mathematically formulated by Raney (1998). They also include the re-alignment of the tracker range commands (the central look of the stack is taken as reference).
- The multi-looking operation is performed on this extended stack, by averaging the 45 single looks in the azimuth direction. Thus, a first UF-SAR mode waveform is obtained in an extended window analysis.
- The window analysis is finally tailored, to restore the nominal 128 sample size. For that purpose, we use the variable “*range_shift_waveform_20_ku*”, available in the ESA L2 product, to select the 128 samples. Therefore, this shift is the same one as applied on-ground to truncate the window analysis (in the ESA PDGS this shift is set to position the waveform main energy peak at sample n°44).

f) Pulse Target Response Convolution

The multi-looked UF-SAR waveforms are oversampled in the range-time domain to be convolved with the radar system Pulse Target Response (PTR_T), with:

$$PTR_T = \left| \frac{\sin \pi \frac{t}{T}}{\pi \frac{t}{T}} \right|^2 \quad (5)$$

where $T = 1/Bw$

After convolution, the UF-SAR waveforms are undersampled to the nominal 128 sample size. It must be noted that, after few unsuccessful tests, it was decided to not apply the Azimuth Impulse Response (AIR) to the DDM. This will be reconsidered in a future processing version.

Section S2: Quantitative assessment of the AMPLI simulated waveforms (section 2.4)

In this assessment, we compare the first peak position in the window analysis between Sentinel-3 UF-SAR waveforms generated by the ESA PDGS, and the ones simulated by AMPLI. The first peak position (i.e. epoch parameter) is estimated with the OCOG/ICE-1 retracker, 50 % threshold. The analysis is performed on the data set presented section 3.1, including Sentinel-3A and Sentinel-3B measurements acquired from 9 May to 25 August, 2019.

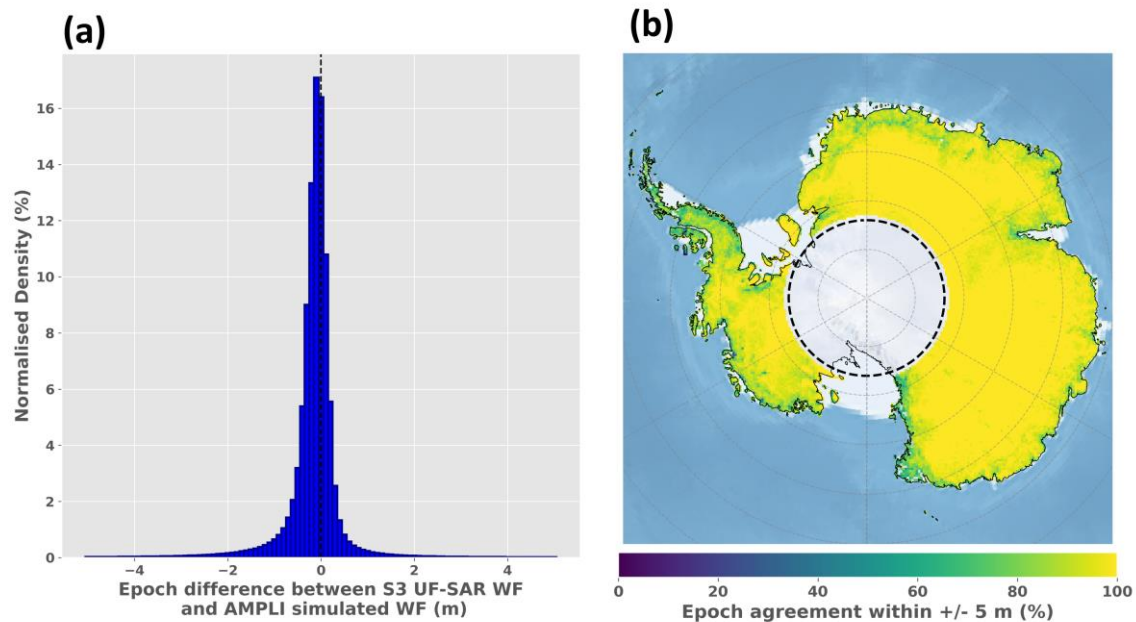


Figure S2: (a) Histogram of the difference in the epoch parameter estimated on the Sentinel-3 UF-SAR measured and simulated waveforms (b) Gridded ratio of measurements from which the epoch parameter estimated on the Sentinel-3 UF-SAR measured and simulated waveforms is within a ± 5 m agreement. Grid resolution is 25 km. 100 measurements minimum per grid points are required for the computation.

Section S3: Additional statistics in the Sentinel-3 and ICESat-2 comparisons (section 3.1)

The following numbers are the total amount of Sentinel-3A and Sentinel-3B measurements analysed in the analysis presented section 3. They were acquired by the satellites from 9 May to 25 August, 2019.

Total amount of Sentinel-3 data:	27 563 782 measurements
After common quality controls:	26 026 408 measurements (94.42%)
After second selection (AMPLI):	25 037 763 measurements (90.84%)
After second selection (ESA L2):	25 429 092 measurements (92.26%)

Note: The percentage under bracket indicates the ratio of measurements relative to the total amount of Sentinel-3 20 Hz measurements

Quality controls, common selection

Quality controls	WF peak detection	SNR	DEM coverage	SUM
Data discarded (%)	4.67%	1.83%	0.73%	5.58%

Table S2: Common quality checks applied to the Sentinel-3 elevations over the Antarctic ice sheet data set. The percentages are relative to the total amount of measurements. In the second table the percentages are relative to the amount of measurements after first selection.

Quality controls, second selection specific to each data set

	Quality controls	deviation to DEM > 50m	relocation distance > 15 km	Retracking or Relocation failures	Surface ambiguities	Agreement data vs simulation	AMPLI relocation failures	SUM
ESA L2	Data discarded (%)	2.14 %	< 0.001%	0.03%	Not applicable	Not applicable	Not applicable	2.17%
AMPLI	Data discarded (%)	< 0.001%	0.87%	Not applicable	2.34%	0.52%	0.88%	3.59%

Tables S3: Quality checks applied to the Sentinel-3 elevations over the Antarctic ice sheet data set. The percentages are relative to the amount of measurements after first selection.

Brief description of quality controls:

- **WF peak detection:** the measurement is discarded if no clear energy peak in the UF-SAR waveform is identified. The peak detection is based on the Leading Edge Detection (LED) algorithm described in Aublanc et al. (2021). For AMPLI, the peak detection is anyway mandatory to estimate the altimeter range, as described in section 2.3. We decided to apply this criteria to ESA L2 measurements, for the sake of fair comparison between both data set.
- **Signal to Noise Ratio (SNR):** A backscatter coefficient (Sigma-0) is computed for all measurements (dB unit), according to:

$$\text{Sigma}0 = 10 * \log_{10}(A_{\max}) + S_f + S_b + C_o$$

where A_{\max} is the maximum amplitude of the Sentinel-3 UF-SAR waveform,

S_f is a scaling factor, read in the Land Ice Thematic Product (variable “*scale_factor_20_ku*”),
 S_b is a systematic bias, applied in the ESA Processor, equal to -0.65 dB,
 C_o a calibration offset, calculated to roughly align this Sigma-0 with the one from the SAMOSA physical retracker (calibration performed over the ocean), equal to -18 dB

The measurement is discarded if the Sigma-0 is lower than -12 dB. In fact, below this threshold we noticed that approximately less than 50% of the waveforms have a clear energy peak (based on the LED algorithm). Therefore, we considered that the measurement is not reliable. This criterion is already used within the Sentinel-3 Mission Performance Cluster (MPC) project, to check the measurement quality over the polar ice sheets.

- **DEM coverage:** the measurement is discarded if the DEM is not 100% complete in the cross-track direction to the nadir point, up to ± 8 km (i.e. REMA value found at “-9999”)
- **Deviation to DEM:** the measurement is discarded if the altimetry elevation deviates by more than 50 meters to the REMA value, 10 m version (the DEM value is bi-linearly interpolated at the point of first radar return coordinates).
- **Relocation distance:** the measurement is discarded if the ground distance between nadir and the estimated point of first radar return is higher than 15 km.
- **Retracking or Relocation failures** (applicable only to ESA L2 elevations). After the first common quality controls, $\sim 0.03\%$ of the remaining range estimations do not have a physical value (in the parameter “*range_ocog_20_ku*”). This is most likely due to failures in the retracking or relocation algorithms.
- **Surface ambiguities** (applicable only to AMPLI elevations only). Ambiguity in the estimated point of first radar return, as described section 2.3. Either because distinct facet clusters contribute to the identified energy peak, with no one found predominant, or because the facet cluster illuminates a surface larger than 6 km in the cross-track direction.
- **Agreement data vs simulation** (applicable to AMPLI elevations only). Two quality controls are performed to check the simulation validity. (1) Firstly, we check the absolute cross-correlation delay between Sentinel-3 UF-SAR waveform and AMPLI simulated waveform remains below 30 range gates (~ 14 m) (2) Secondly, after cross-correlation, we check a waveform leading edge is detected in the AMPLI UF-SAR simulated waveform using the LED algorithm. The position of this waveform leading edge must be relatively close to the one detected in the Sentinel-3 UF-SAR mode waveform (maximum delay allowed is 12 range gates ~ 5.6 m).
- **AMPLI relocation failures** (applicable to AMPLI elevations only). They correspond to measurements for which no energy is found in the CrossTrack Backscattered Distribution (CTBD) signal. These errors are detected for $\sim 0.88\%$ of the measurements (after first common quality controls) and will be investigated in the future.

Section S4: Data sampling over Pine Island drainage basin (section 3.1)

Illustration of the data sampling achieved over Pine Island drainage basin, with AMPLI processing applied to Sentinel-3A (green) and Sentinel-3B (blue) measurements, after data editing presented section S3. One orbit cycle of both satellites is displayed, $n^{\circ}47$ and $n^{\circ}27$ respectively for Sentinel-3A and Sentinel-3B (corresponding to measurements acquired during the Antarctic winter 2019). The topography is estimated at the point of first radar return, which explains the non-linear paths on-ground.

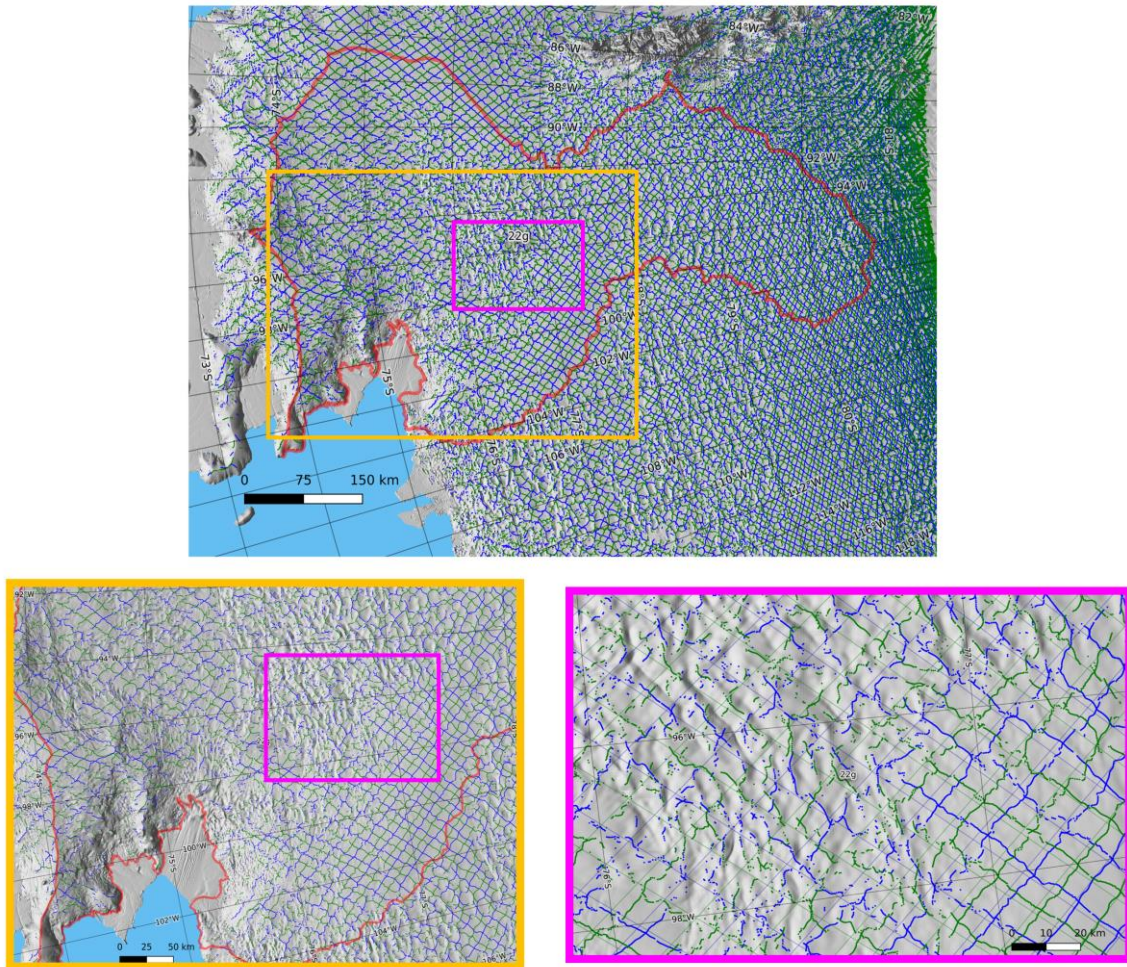


Figure S3: Data sampling over Pine Island drainage basin (red outline) with AMPLI processing applied to one orbit cycle of Sentinel-3A (green) and Sentinel-3B (blue) measurements. Yellow and magenta boxes are zoom views of the top figure.

Section S5: Alternative Sentinel-3 SEC computation (section 4.2)

To confirm the validity of the Sentinel-3 Surface Elevation Change (SEC) presented in this study (section 4.4), the SEC was calculated with an alternative method. It is based on differences between Sentinel-3 and ICESat-2 ATL06 nearly co-located measurements in space and separated by 3 years in time. The method comprises the main operations:

- 1) Computation of surface elevation difference between Sentinel-3 and ICESat-2 ATL06 measurements separated by 3 years (+/- 46 days). With Sentinel-3 measurements acquired from 9 May to 25 August, 2019.
- 2) The elevation differences are gridded in a polar stereographic projection, 20 km resolution, same grid coordinates as ICESat-2 ATL15 products. 30 nearly co-located measurements were required for the computation. This provided an initial estimate of the gridded SEC.
- 3) In order to remove the initial bias between the two missions, the same computations and same grids are calculated with Sentinel-3 and ICESat-2 ATL06 nearly co-located measurements (in space **and time**), acquired in 2019.
- 4) The final gridded SEC is obtained by subtracting the “calibration grid”, to the initial SEC grid (step 2 grid – step 3 grid).

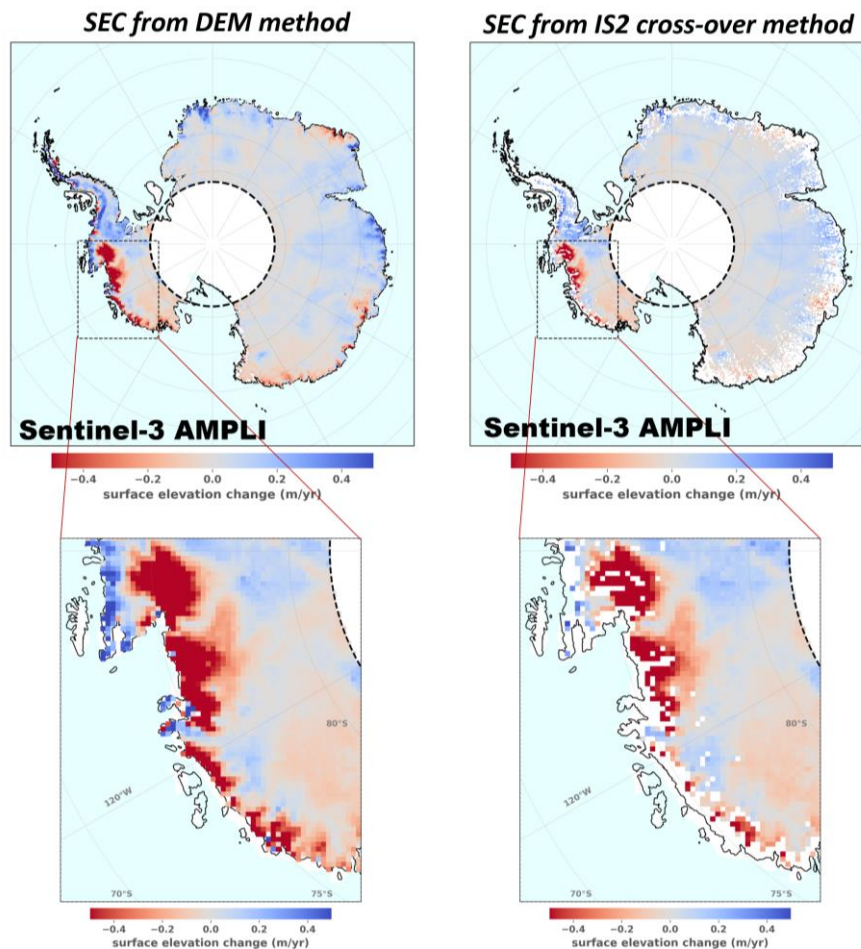


Figure S4: (a) Surface Elevation Change (SEC) of the Antarctic ice sheet over the 2019–2022 period. The SEC is estimated with Sentinel-3A and Sentinel-3B measurements processed by AMPLI, using the DEM method presented section 4.4 (left) and with an alternative method performed through cross-over to ICESat-2, as presented in this supplementary material (right). Grid resolution is 20 km.

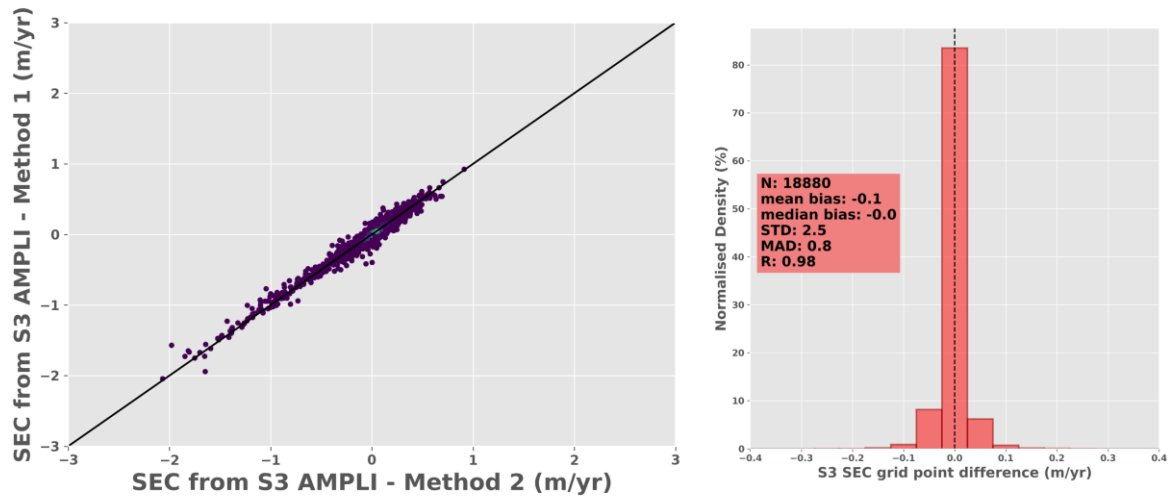


Figure S5: (a) Scatter plot of the SEC grid point differences, as estimated with Sentinel-3 through the DEM method presented section 4.4 (method 1), and with the ICESat-2 cross-over method, as presented above in this supplementary material (method 2). (b) Histogram of the grid point differences.

Section S6: Sentinel-3 AMPLI and ICESat-2 elevation differences in the Antarctic ice sheet interior (section 5.1)

In this section, we complement the investigations made in the East Antarctic Ice Sheet (EAIS) interiors, related to snow volume scattering effect.

The two first figures below (Fig. S6a and Fig. S6b) show the gridded median elevation bias between surface height estimates from Sentinel-3 AMPLI and ICESat-2 ATL06. As described in section 5.1, the analyses are restricted to the East Antarctic Ice Sheet (EAIS) interiors, where surface elevation is above 2,500 meters, surface slope is below 0.2° and SEC is below 5 cm yr^{-1} in the 2019-2022 period (according to ICESat-2 ATL15 product). Fig. S6a is the same result as presented in section 3, with Sentinel-3 and ICESat-2 measurements acquired in 2019 (except for the geographical selection). Fig. S6b is the equivalent analysis, made with Sentinel-3A and Sentinel-3B measurements acquired in 2022 (data set used for the SEC computation, presented section 4.1). As written in section 5.1, the elevation bias between Sentinel-3 and ICESat-2 ATL06 depict spatial variations, that are differently distributed in space between 2019 and 2022 analysis.

Fig. S6c shows the difference between maps in Fig. S6b and Fig. S6a (divided by a factor of 3, to convert into m yr^{-1} unit). Fig. S6d displays the Sentinel-3 SEC estimated with Sentinel-3 in this study over the analysis region (extracted from the global map shown in Fig. 7). The two maps, Fig. S6c and Fig. S6d, are in high correlation, with a ~ 0.95 Pearson Correlation Coefficient between the map grid points. Because the surface topography is assumed stable in this area ($\text{below } 5 \text{ cm yr}^{-1}$), this most likely indicates that the SEC estimated by Sentinel-3 over this region is artificially driven by the snow volume scattering. This result emphasizes the need for a snow volume scattering correction, as discussed in section 6.2.

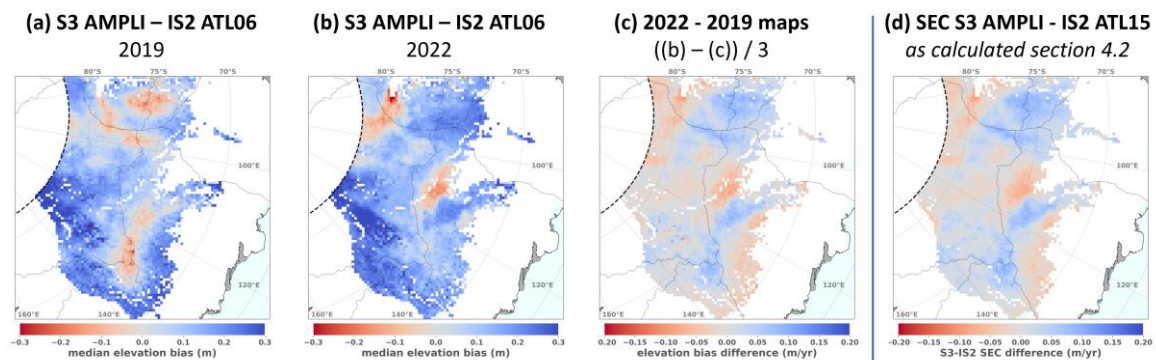


Figure S6: (a) Gridded statistics of the median elevation bias between Sentinel-3 and ICESat-2 ATL06 co-located elevations, for measurements acquired in the 2019 Antarctic winter (b) Same map with Sentinel-3 and ICESat-2 measurements acquired in the 2022 Antarctic winter (c) Difference between the two first maps, divided by a factor of 3 to convert in m yr^{-1} unit (d) 2019-2022 SEC of the Antarctic ice sheet calculated in the frame of this study with Sentinel-3 AMPLI. The analysis is performed over the ice sheet interior (surface elevation above 2,500 meters, surface slope below 0.2° and ICESat-2 ATL15 SEC below 5 cm yr^{-1}). Grid resolution is 20 km.

Section S7: Illustration of AMPLI simulation over the Antarctic ice sheet interior (section 5.3)

Fig. S7 is a figure equivalent to Fig. 1 (in the main text), but for a Sentinel-3A measurement acquired in the East Antarctic ice sheet interior. The surface slope is estimated at 0.05° . Fig. S8 below displays the Sentinel-3 and the AMPLI UF-SAR waveforms for this measurement. Waveform shape differences are mainly observed in the trailing edge part. We assume this is because snow volume scattering is not yet included in the modelling.

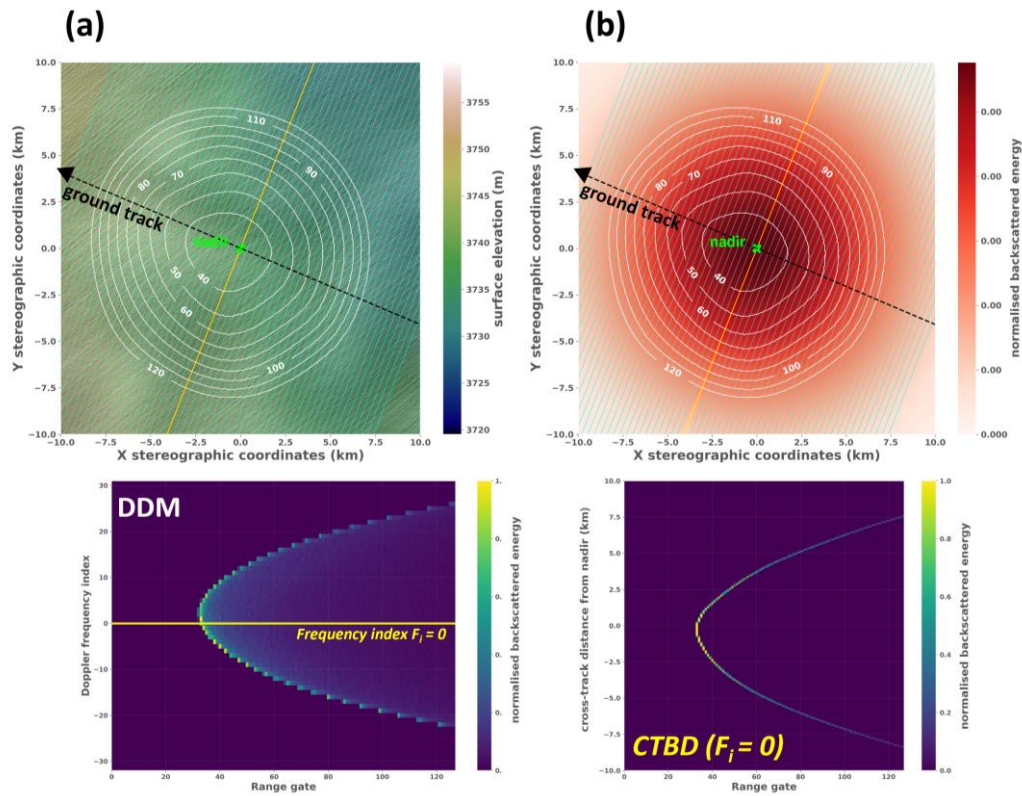


Figure S7: Same plots as Fig. 1 in the publication, but for a Sentinel-3A measurement acquired in the East Antarctic ice sheet. (a) Topography from REMA, over which the simulation is performed (only a 20 km x 20 km area is represented). The white contours display the iso-range lines R_i , the cyan lines represent the 64 delay-Doppler frequencies (b) Energy backscattered at snow-air interface P_f s (c) Delay-Doppler Map simulated by integrating the energy P_f s, given the satellite-facet distance in slant range and in along-track (d) Cross-Track Backscatter Distribution, showing the histogram of the energy P_f s in the cross-track direction, along for the Doppler frequency index $n=0$.

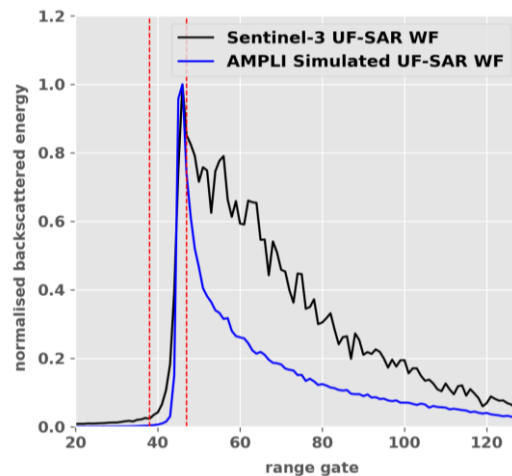


Figure S8: Simulated (blue) and measured (black) Sentinel-3 UF-SAR waveforms for the same measurement as shown in Fig. S7.